On energy harvesting from a vibro-impact oscillator with dielectric membranes

Z. H. Lai[a,c,d], G. Thomson[a,*], D. Yurchenko[a], D. V. Val[b], E. Rodgers[a]

[a]IMPEE, Heriot-Watt University, Edinburgh, EH14 4AS, UK

[b]Institute for Infrastructure & Environment, Heriot-Watt University, Edinburgh, EH14 4AS, UK

[c]School of Mechatronics Engineering, Nanchang University, Nanchang, 330031, People's Republic of China.

[d]Key Laboratory of Lightweight and high strength structural materials of Jiangxi Province, Nanchang University, Nanchang 330031, People's Republic of China

*Corresponding author. Email address: grt2@hw.ac.uk

Abstract:

A vibro-impacting mechanical system comprising a ball moving freely between two dielectric membranes located at a certain distance from each other is studied. When impacting interactions between the ball and the membranes occur the device generates energy harvested from ambient vibrations. The energy harvesting principle of the proposed system is formulated and used to numerically estimate its output voltage. The dynamic behavior and output performance of the system are thoroughly studied under a harmonic excitation, different initial conditions and various values of the restitution coefficient of the membranes. The research results are useful for selecting the system parameters to achieve an optimal output performance in a realistic vibrational environment.

Keywords:

Non-linear energy harvesting; dielectric elastomer; vibro-impact ; bouncing ball

1 Introduction

Energy recovered from various sources of ambient vibrations is considered to be renewable, clean and can be converted into electricity[1]. The energy harvesting (EH) devices utilizing ambient vibrations require a small size, high energy density and low cost especially in applications such as automotive[2,3], aeronautical[4], wireless sensors networks[5,6], wearable devices[7] and other sectors[8-10].

There are three mainly conventional transduction methods converting vibrational energy to electrical one: electromagnetic, electrostatic and piezoelectric, whereas a triboelectric effect has rapidly been gaining its popularity. The transduction process of electromagnetic (EM) EH is based on Faraday's law of induction. Poor scaling qualities make EM EH unfeasible for micro scale applications where it can only provide a quite small voltage output, while for large scale applications such devices become heavy and bulky. Moreover, due to the dependence of the induced voltage on the relative velocity of a magnet and coils, the larger size applications, like linear generators for wave energy converters, have not been very successful so far. Electrostatic (ES) EH is based upon the use of a variable capacitor with one fixed plate and one plate connected to a vibrating body. Its advantages and disadvantages are both related to the requirement for an input voltage. Since the output voltage is quadratically proportional to it, the larger the input voltage the higher the energy gain. The majority of investigations on EH from ambient vibrations so far have been focused on the use of piezoelectric (PZT) materials[11-15]. These PZT EH devices have simple structure and relatively high energy conversion efficiency. However, these devices can only work within a limited frequency for a special type of motion[16] and produce relatively small power density. These factors greatly restrict the areas of application of PZT EH devices.

In recent years, dielectric elastomers (DEs) have shown their advantages for vibrational energy conversion and attracted much attention from researchers. DE generators[17-20] are fabricated using highly flexible elastic materials (such as acrylic, silicones, polyurethanes, etc.), sandwiched between flexible electrodes that convert mechanical work to electrical energy. DE-based generators can convert linear, nonlinear or rotational motion under a wide frequency range[21]. DEs also possess such advantages as a low mass density, large deformability, high energy density, rather good electro-mechanical conversion efficiency, moderate or low cost, solid state monolithic embodiment with no sliding parts, good chemical resistance to corrosive environments, silent operation, as well as easiness to manufacture and recycle[22]. Therefore, DEs have significant potential in EH from vibrational energy due to their ability to work at micro scale, diversity of structure, etc.

To convert vibrational energy into electrical one DE acts as a variable capacitance capacitor. A DE generator was first proposed by Pelrine et al. back in 2001[23]. Suo et al.[24] established the DE theory based on thermodynamics and continuum mechanics. Following their work, many researches related to DE generators have been published. The basic material properties, failure mechanisms and identification methods have been studied[25-27]. A detailed model that describes the four cycling phases of DE-based EH was developed in [28], whereas the influence of the material dielectric coefficient on the EH performance and bias voltage was considered in [29]. These researches have emphasized that major advantages of DE-based generators are their high energy density (up to 0.4 J/g), which is at least an order of magnitude higher than the specific energies of EM, ES and PZT generators[30], especially at low frequencies, and high stretching capabilities. The highest power density that has been achieved with DE is up to 3.8 $\mu W/mm^3$[5], which is much higher compared to EM (2.21 $\mu W/mm^3$[31]), ES (2.16 $\mu W/mm^3$[32]) and PZT (0.375 $\mu W/mm^3$[33]). These researches have demonstrated the benefits of using DEs in EH and laid the foundation for further investigations of DE-based EH systems.

The main principle of DE EH is based on the deformation of a DE material in or out of plane by applying either an external force or pressure, depending on the design and application of the DE generator. For instance, in a novel wave energy converter (WEC)[34] a DE material is stretched by pressured air pushed into a chamber by waves, which is similar to the oscillating water column principle. Another idea of a WEC that utilizes a DE material and harness energy of surge motion has recently been reported[35]. Many papers are currently available on the material properties of DEs[25,27]; however, only a few works have studied various concepts of DE-based generators and their performance that limits the application of DE for vibrational EH in real life. Therefore, there is a clear need for further study of DE-based generators and their EH performance under simulated or natural ambient vibrations.

Irrespective of a conversion method used, it is apparent that the effectiveness of a parametric[36] or nonlinear[37] energy harvesting is higher than that of a linear system in realistic environmental conditions, where the excitation frequency is not fixed. Dynamic systems with a vibro-impact (VI) interaction[38-43] belong to a class of strongly nonlinear systems that are used in various machines[44,45] and can be used as vibro-impact dampers and nonlinear energy sinks[46-49]. Impacts are usually associated with high kinetic energy, which can be harnessed. Usually VI systems consist of a mass-spring element colliding against a motionless stopper, but in some advance cases a motion of two mechanical systems is coupled through impacts[50]. Apparent difficulty in dealing with a VI motion comes from very rich, complex and highly nonlinear behavior and bifurcation pattern[51] of such systems that should be studied numerically for each and every new layout. Several layouts of VI

EH devices have been reported based on PZT material[52-55] and electromagnetics[56], whereas a DE-based dynamical VI system consisting of a bouncing ball on a vibrating workbench[57,58] was studied in our previous work[59,60].

Our previous studies of the DE EH device were focused on the introduction and basic analysis of the system, whereas the restitution coefficient between the membrane and the ball was, for simplicity, set to unity. Building on those works, the dynamic behaviors and the EH performance of the DE-based dynamical VI system are further studied in this paper. Results of the study can be used to optimize the device design. The basic principles of EH using the DE-based device are introduced in Section 2. The dynamic behavior and EH performance of the device for different initial conditions as a function of excitation amplitude and frequency are thoroughly studied in Section 3. A discussion of how the results can be used to optimize the device performance in a real vibrational environment, including an illustrating example, is presented in Section 4. Conclusions are drawn in Section 5.

2 Basic principles

The principle of power generation by a DE generator relies on increased capacitance due to mechanical deformation of the elastomer. In order to convert vibrational energy into electrical one by taking advantage of DE, an inclined vibro-impact model has been presented[60], as shown in Figure 1. The system comprises a cylinder, an inner ball sliding freely inside the cylinder and two pre-stretched circular DE membranes at both ends of the cylinder. Both pre-stretched membranes are sandwiched between compliant electrodes and wires are connected to both sides of each membrane. Each membrane is fixed between two identical cylindrical frames and then connected to the cylinder. The system is inclined with an angle of β ($0° \le \beta \le 90°$) between the direction along its symmetry axis (denoted as z-direction in this paper) and the horizontal plane. The case of $\beta = 90°$ is identical to the case of bouncing ball on a harmonically oscillating surface that has been studied quite intensively in [57,58]. The system can move freely in the z-direction subject to an external excitation $F(t)$.

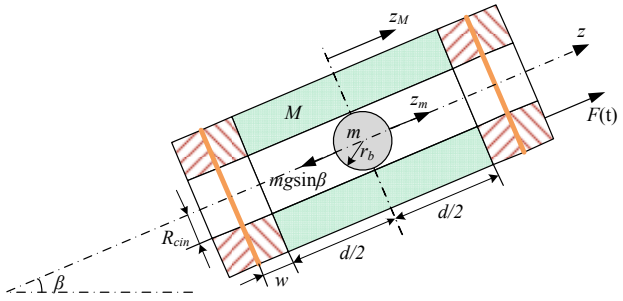

Figure 1. Sketch of the proposed DE-based dynamic vibro-impact system

In this model, the mass of the outer structure (the system without the inner ball) is denoted by M and the mass of the inner ball by m. The inner radius of the cylinder is R_{cin}, the radius of the ball is r_b which is a little smaller than R_{cin}. The active radius of both circular pre-stretched membranes is R_0 (= R_{cin}) and thickness h_0. U_{in} denotes an input voltage applied to the membranes. The length of the cylinder is d whereas the cylinder frames' width is w. The cylinder is excited by an external excitation $F(t)$ applied along the z-direction, and z_M and z_m are the displacements along z

-direction of the outer structure and inner ball respectively, as shown in Figure 1. The origin of the coordinate system for the inner ball coincides with that of the cylinder and is set in the middle of the cylinder. The friction between the inner ball and the cylinder is quite small and ignored for unrestricted motion of the ball. The output voltage of the system is denoted as U_{out}, which is equal to the larger voltage across the two membranes when they are connected in parallel to an energy harvesting circuit.

Suppose a harmonic excitation $F(t)=A\cos(2\pi f_0 t)$ is applied to the system, where A and f_0 denote its amplitude and frequency, respectively. Due to a low mass ratio of the inner ball to the outer structure and direct excitation of the cylinder, impacts are assumed to have little or no effect on the outer structure. The outer structure moves under the excitation as following:

$$z_M''(t) = F(t)/M = \frac{A}{M}\cos(2\pi f_0 t) \tag{1}$$

Thus, the displacement and velocity of the cylinder between the impacts can be easily obtained:

$$\begin{cases} z_M'(t) = \dfrac{A}{M(2\pi f_0)}\sin(2\pi f_0 t) + C \\ z_M(t) = -\dfrac{A}{M(2\pi f_0)^2}\cos(2\pi f_0 t) + Ct + D \end{cases} \tag{2}$$

where the values of C and D depend on the initial conditions of the cylinder.

The inner ball, in its turn, experiences the gravity component $-mg\sin\beta$ ($g = 9.8$ m/s^2 represents the gravitational acceleration) and moves freely inside the cylinder until it impacts one of the membranes:

$$z_m''(t) = -g\sin\beta \tag{3}$$

Introduce the relative displacement $\Delta z = z_m - z_M$ as the difference between z_m and z_M, and $s = d + 2w - 2r_b$ as the largest distance the ball can cover inside the cylinder without the impact. Thus, impacts between the ball and one of the membranes occur under the following conditions:

$$\begin{cases} \Delta z = z_m - z_M = -s/2,\ z_m' < z_M' & \text{when the ball impacts the left/bottom membrane} \\ \Delta z = z_m - z_M = s/2,\ z_m' > z_M' & \text{when the ball impacts the right/top membrane} \end{cases} \tag{4}$$

Denote the limit left (bottom) and right (top) positions of the ball inside the cylinder as $z_L(t) = z_M(t) - s/2$ and $z_R(t) = z_M(t) + s/2$ correspondingly, then (4) becomes:

$$\begin{cases} z_m = z_L,\ z_m' < z_M' & \text{when the ball impacts the left/bottom membrane} \\ z_m = z_R,\ z_m' > z_M' & \text{when the ball impacts the right/top membrane} \end{cases} \tag{5}$$

The dynamic of the ball is changed after each impact accordingly. Let v_{m-} and v_{m+} represent the velocities of the ball just before and after each impact, and v_{M-} and v_{M+} the velocities of the outer structure before and after each impact, respectively. In view of the previous assumption of the small mass ratio and the cylinder directly driven by the external force the cylinder velocity is kept constant $v_M = v_{M-} = v_{M+}$. When impacts occur the varying elastic force of the membrane $f(x)$, where x represents the deflection of the membrane, will produce negative work onto the ball until it reaches the largest deflection δ, at that moment the velocity of the ball becomes equal to v_M. Considering

the outer structure as the reference frame, the following equation can be written according to the conservation of energy theorem:

$$0-\frac{1}{2}m\left(v_{m-}-v_M\right)^2=\int_0^\delta\left[-f\left(x\right)\right]dx \tag{6}$$

where

$$f(x)=Kx^n \tag{7}$$

represents the elastic force, whose relationship with x has been obtained experimentally and reported in our previous work[59]. Therefore, the largest deflection of the membrane at impacts can be obtained as:

$$\delta=\left[\frac{n+1}{2K}m\left(v_{m-}-v_M\right)^2\right]^{\frac{1}{n+1}} \tag{8}$$

At the maximum deformation the membrane achieves its maximal area A' and minimal thickness h'. The area of the membrane at this moment consists of two parts[59]:

$$A'=A_1'+A_2' \tag{9}$$

where

$$\begin{cases} A_1'=2\pi r_b(r_b-r_b\cos\alpha)=2\pi r_b^2(1-\cos\alpha) \\ A_2'=\dfrac{\pi R_0^2-\pi(r\sin\alpha)^2}{\cos\alpha} \end{cases} \tag{10}$$

The value of α is determined by deflection δ and sizes of the cylinder and the ball:

$$\cos\alpha=\frac{-2r_b\left(\delta-r_b\right)+2R_0\sqrt{R_0^2+\delta^2-2\delta r_b}}{2\left[R_0^2+\left(\delta-r_b\right)^2\right]} \tag{11}$$

Apparently, the membrane's area A' increases when δ increases and due to the membrane's incompressibility its thickness decreases. The thickness of the membrane at its largest deflection can be written as:

$$h'=\frac{\pi R_0^2 h_0}{A'} \tag{12}$$

Thus, the minimal capacitance of the deformed membrane at its original shape and the maximal one at its largest deformation in one impact can be obtained as:

$$C_0=\frac{\varepsilon_0\varepsilon_r A_0}{h_0}=\frac{\varepsilon_0\varepsilon_r V}{h_0^2} \tag{13}$$

$$C'=\frac{\varepsilon_0\varepsilon_r A'}{h'}=\frac{\varepsilon_0\varepsilon_r V}{h'^2} \tag{14}$$

where ε_0 is the vacuum permittivity, ε_r is the relative permittivity of the DE material, and V is the constant volume of the membrane. Therefore, the output voltage of the membrane at impacts can be further obtained[59,60]:

$$U_{imp} = \frac{C'}{C_0} U_{in} = \frac{h_0^2}{h'^2} U_{in} \tag{15}$$

Because each membrane serves as variable capacitor, one arrives to the well expected result (15), where $h' < h_0$; consequently, the voltage not only bigger than the input one $U_{imp} > U_{in}$, but also is proportional to it. Hence, the output voltage of the system $U_{out} = U_{imp}$ when impacts occur, and U_{out} is simply equal to U_{in} at any other time. Therefore, the external vibrational energy can be converted to electric one through the ball's impacts by using the presented dynamic model. The voltage gain is $\Delta U = U_{imp} - U_{in} = [(h_0 / h')^2 - 1]U_{in}$, which can be increased by increasing the input voltage, which is the main advantage of variable capacitor devices.

The velocity of the ball after an impact can be calculated as[57]

$$v_{m+} = \frac{1+r}{1+\mu} v_M + \frac{\mu - r}{1+\mu} v_{m-} \tag{16}$$

where r is the restitution coefficient of the membrane, and $\mu = m / M$ is the mass ratio of the inner ball to the outer structure. When M ? m, μ can be regarded as 0 and (16) can be simplified as:

$$v_{m+} = -r v_{m-} + (r+1) v_M \tag{17}$$

It should be stressed that the nonlinear mechanical property of the membranes is not used for the dynamic evaluation of the ball velocity at/after impact, but rather exploited for estimating the membrane deformation and voltage output. The mechanical interaction of the cylinder and ball is governed by the Newton's impact law rewritten in form (16) and (17). An ideal case of a purely elastic impact $r = 1$ has some theoretical interest, whereas the case of an inelastic impact $0 < r < 1$ is more practical. Apparently, in the case of elastic impact the ball evolution will be determined by initial conditions (and the excitation parameters, of course), while in the case of inelastic impact ($0 < r < 1$ may be considered as a "concentrated" in time dissipative force) the influence of initial conditions will gradually disappear with time. Nevertheless, it is important to understand the influence of initial conditions because in such a nonlinear system they may force the system to a certain behavior.

After an impact the ball will move freely until next impact and this process will repeat itself again and again. Based on the previous analyses, the displacements and velocities of the outer structure and the ball can be obtained at any time provided the external excitation of the system and initial conditions are specified.

The higher output voltages can be harvested as electrical power through a simple EH circuit that has been studied and reported[59]. The electrical power can be easily calculated from the output voltages, therefore, the system output voltage is a key parameter to evaluate the EH performance of the system: the higher the output voltage, the more electrical energy is harvested. According to the above analysis, one can see that the system output voltage is governed by the dynamic interaction between the cylinder and the ball as well as the electrical and mechanical properties of the membrane. The latter one has experimentally been validated at our previous work[60]. Therefore, the EH performance of the proposed system under different input parameters can be reasonably evaluated based on its dynamic analysis, which can only be obtained through numerical simulations due to the complexity of the nonlinear system.

3 Numerical simulations

The dynamics of the presented system is extremely complex and rich due to its nonlinearity. In order to fully reveal the dynamic behaviors and EH performance of the proposed system, the 4th Runge-Kutta algorithm with time step 10^{-5} s is adopted in this paper to solve the differential equations and obtain the system response under pure harmonic excitation. The following set of parameters was used for numerical simulations in this paper unless otherwise stated: M=124.5 g, $m=3.5$ g, the membranes are twice pre-stretched with $R_0=R_{cin}$=6.3 mm, $h_0=0.25$ mm, $r_b=5$ mm, $d=42$ mm, $w=6$ mm, $U_{in}=2000$ V, whereas $K=4.0847\times10^5$ and $n=2.6$ are set in (7) according to previous experiments[59].

A set of specific parameters are selected first to illustrate the system response: $\beta=0°$, $r=1$, and the initial conditions of the system are set at $z_M(0)=-A/[M(2\pi f_0)^2]$, $z'_M(0)=0$, $z_m(0)=z_M(0)+s/2$ ($z_m(0)>0$) and $z'_m(0)=-4f_0z_m(0)$. It is easy to imagine that the ball will periodically impact both membranes when the velocity of the cylinder is at zero so that the ball's motion looks like a saw-tooth signal, that is shown in Figure 2 for $A=0.1$ N and $f_0=2$ Hz. Figure 2(a) presents the ball displacement (blue) and membranes' motion (red); one can clearly observe a "pure" or "classical" vibro-impacting regime with consequent impacts against each membrane that is reflected in the sharp peaks and troughs. The velocities of the cylinder and the ball are presented in Figure 2(b) where one can see the velocity of the ball reverses at impacts when $z'_M=0$. The impacts, which occur when $z_m=z_L$ or $z_m=z_R$ according to Figure 2(a), will produce extra voltage, shown in Figure 2(c), which in this particular case is the same for each impact. Figure 2(d) presents the phase trajectory of the ball in a steady-state case (50~100 s in this paper), after all the transient oscillations died out. Single closed trajectory indicates a simple periodic motion of the ball, as expected.

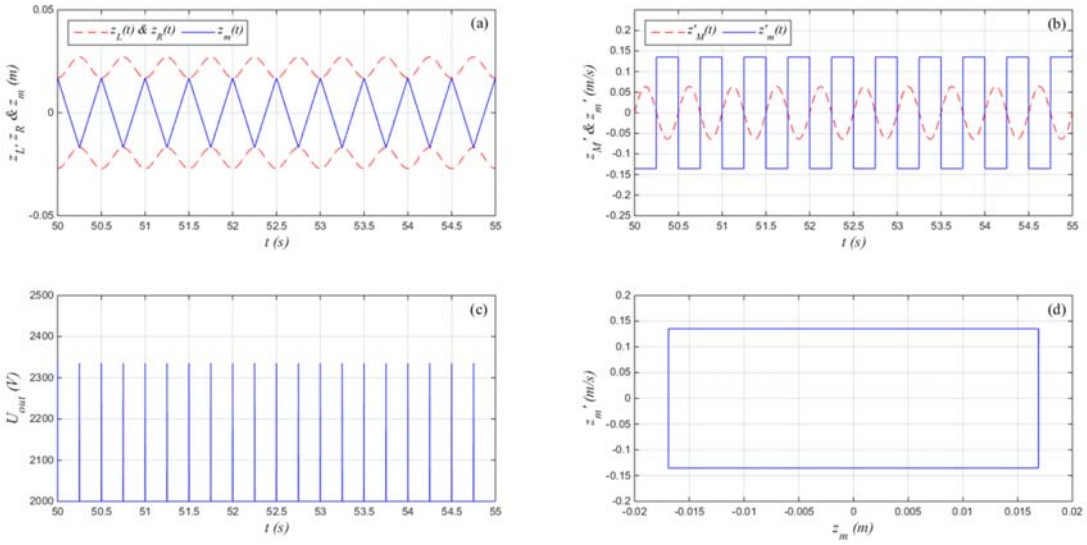

Figure 2. (a) Displacements and (b) velocities of the outer structure and the ball, (c) output voltage versus time for β=0°, $r=1$, A=0.1 N and $f_0=2$ Hz under saw-tooth initial conditions, and (d) the ball's phase trajectory.

However, this ideal saw-tooth pattern can be easily destroyed when $\beta>0$ or $r<1$ or the initial

conditions are not satisfied. Therefore, it is necessary to further discuss the influence of all relevant parameters on the system output performance. These parameters include the initial conditions $x_m(0)$ and $x'_m(0)$, the system parameters β and r, and the excitation parameters A and f_0. It should be pointed out that the initial conditions of the cylinder are set at $x_M(0)$=0 m and $x'_M(0)$=0 m/s in the following discussion, except of some specially mentioned cases. It is easy to calculate that C=0 and $D=A/[M(2\pi f_0)^2]$ in (2).

The harvested electrical power can be easily calculated from the output voltage gain. As stated in Section 2, this voltage depends on the largest deformation of the membranes, whose properties are given and kept constant in this study. Thus, the deformation itself depends on the relative velocity $\Delta v = v_{m-} - v_{M-}$ at the beginning of impacts, assuming that the cylinder motion remains unchanged under the external excitation. To better analyze and compare the system output performance, the overall amount of gained voltages at a steady state (the time interval of 50 to 100 s is selected in this paper to avoid the transient process) is defined as:

$$U_{gain} = \sum_{i=1}^{N} \left(U_{imp}^{(i)} - U_{in} \right) \tag{18}$$

where $U_{imp}^{(i)}$ denote the output voltage of the system at ith impact, and N is the number of impacts within the same time interval. The average gained voltage of the proposed device at its steady state can be defined as:

$$\langle U \rangle_T = U_{gain} / T \tag{19}$$

where T=50 s. To avoid its dependence on the frequency of response and estimate the energy generated at every impact, it is also reasonable to report an average value of voltage gain over a given time interval normalized to the number of impacts:

$$U_{ave} = U_{gain} / N \tag{20}$$

Thus, (19) can be used to estimate the overall EH performance of the proposed device, while (20) helps to understand the system response based on dynamic analysis.

3.1 Influence of the ball's initial conditions

It should be pointed out first that it is impossible to set specific initial conditions in a real life application, especially for the ball which is inside the cylinder and cannot be controlled. Moreover, when $\beta > 0$ the ball will most realistically be resting at the left (bottom) membrane, thus the corresponding initial conditions for the ball are $z_m(0) = -s/2$ and $z'_m(0) = 0$ denoted below as real-ICs[60]. However, in order to fully reveal the nonlinearity of the presented system, a study of the influence of the ball's initial conditions is necessary.

Figure 3(a) presents the U_{ave} under different ball's initial conditions with β=0°, $r = 1$, A=5 N and $f_0 = 2$ Hz. The initial displacement of the ball is between $-s/2$ and $s/2$ physically, and the initial velocity of the ball varies from -5 m/s to 5 m/s. It can be seen that the values of U_{ave} are approximately symmetric in z'_m, and the values rise with an increase in the absolute value of the initial velocity. This indicates that the higher initial kinetic energy of the ball, the higher U_{ave} because there are no energy losses in the elastic impact case ($r = 1$). It can also be seen that the larger the positive initial displacement of the ball, the higher U_{ave} because the cylinder initially moves to

the right $F(t)=A\cos(2\pi f_0 t)$ resulting in a larger velocity at the first impact and later repeated impacts. The contours of Figure 3(a) are plotted in Figure 3(b), where the contours for U_{ave} at 10 kV, 20 kV, 30 kV and 40 k V are presented.

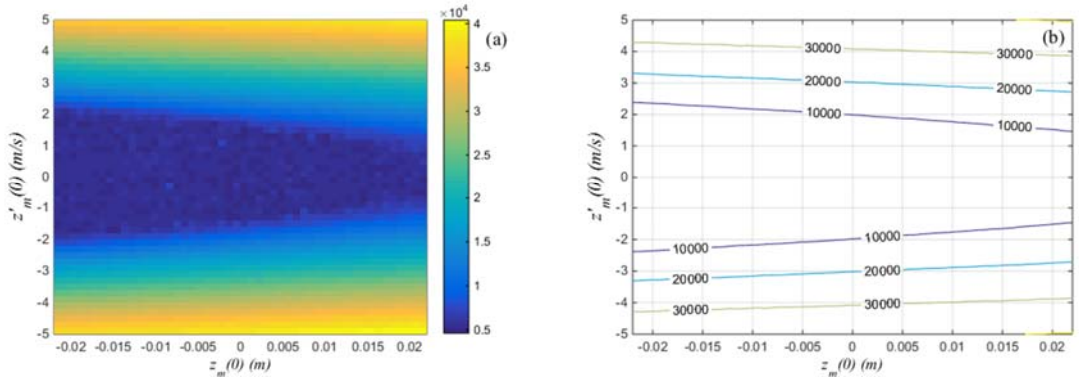

Figure 3. (a) U_{ave} of the presented system under different initial conditions of the ball and (b) the relevant contours for β=0°, $r=1$, A=5 N and $f_0=2$ Hz.

By keeping other parameters the same as those in Figure 3 and setting the values of β at 0°, 30°, 45°, 60° and 90°, the contours of the U_{ave} under different ball's initial conditions are plotted in Figure 4(a). It can be seen that all contours under different β have a similar trend and differences between different angles are quite small, which indicate that the inclinational angle β has little influence on the voltage output under the given system and excitation parameters. This can be explained that if the amplitude of the external excitation is much larger than the gravity component, the excitation is the dominant factor determining the ball's motion and system output while the inclinational angle of the system has little influence. The similar contours under A=20 N are presented in Figure 4(b), where one can see the same trend as that in Figure 4(a). Furthermore, one can see that the curves for low values of initial velocities are denser, locating closer to each other, than that for high value of the initial velocities.

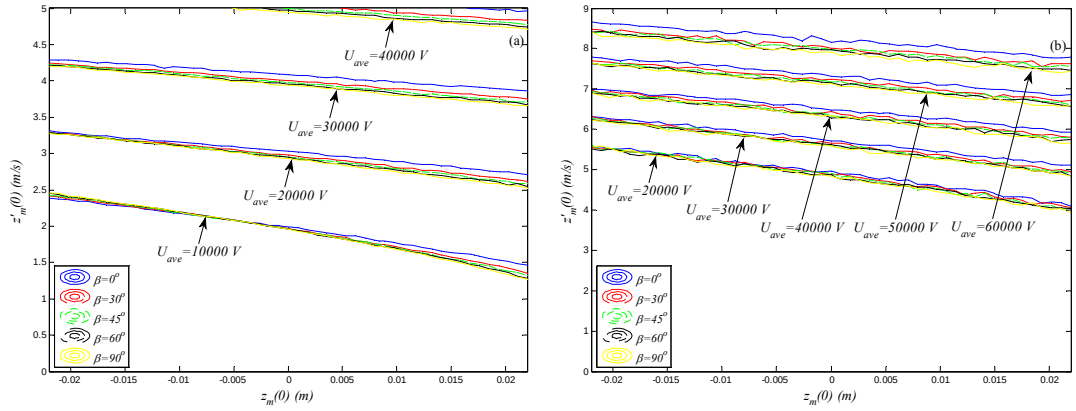

Figure 4. The contours of U_{ave} under different ball's initial conditions when β is set at 0°, 30°, 45°, 60° and 90°, $r=1$, $f_0=2$ Hz and (a) A=5 N; (b) A=20 N.

However, the value of the restitution coefficient r has significant influence on the system output. As noted in Section 2, when $0<r<1$ the initial conditions of the ball barely affect the ball's motion at its steady state. Figure 5 demonstrates the result for U_{ave} under different initial conditions of the ball and two values of the restitution coefficient $r=0.75$ and $r=0.5$. It can be seen from Figures 5(a) and (b), which correspond to the cases of $r=0.75$ and $r=0.5$, respectively, the values of U_{ave} are distributed uniformly over the state space and has values of 4559~4766 V when $r=0.75$ and no gain when $r=0.5$. These results indicate that the inelastic impacts ($0<r<1$) between the ball and membrane will result in dissipation of the ball energy and eliminate the influence of initial conditions on the voltage output. It should be stressed that lower values of r do not directly imply lower levels of gained energy, as one can see later, since the response heavily depends on the excitation frequency.

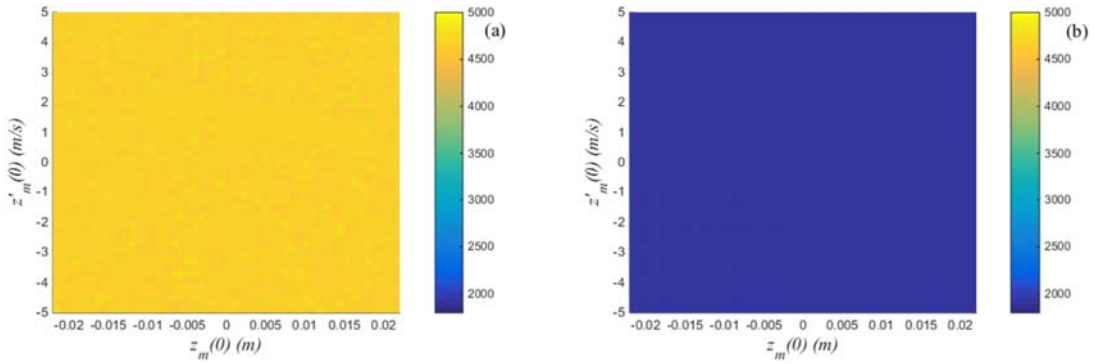

Figure 5. U_{ave} of the system under different initial conditions of the ball when (a) $r=0.75$ and (b) $r=0.5$. β=0°, A=5 N and $f_0=2$ Hz.

Furthermore, the value range of $\langle U\rangle_T$ under different ball's initial conditions is shown in Table 1 for different values of β and r. It can be seen that for a given β, as the value of r decreases, the value of $\langle U\rangle_T$ decreases accordingly due to a larger energy dissipation, which is in general can be seen as a pattern, but for some values of the excitation frequency this pattern may be broken. However, for a given r small enough ($r=0.5$ and $r=0.25$), the values of $\langle U\rangle_T$ under different β are close, which indicates that the values of β have little influence on the system response. It should be noted that for values of r not small enough or close to unity ($r=0.75$ in Table 1) the influence of β on the system response may still exist.

Table 1. The value range of $\langle U\rangle_T$ under different ball's initial conditions for varying values of β and r when A=5 N and $f_0=2$ Hz.

	Output voltage gain per second V/s ($\times 10^4$)				
	β=0°	β=30°	β=45°	β=60°	β=90°
$r=0.75$	7.77	7.65	7.8	7.45	6.37
$r=0.5$	6.21	6.21	6.20	6.18	6.16
$r=0.25$	4.40	4.41	4.42	4.43	4.43

It should be pointed out that an elastic impact is an ideal case that can hardly be encountered in real life, especially since the impacting membranes are soft. Therefore, it is reasonable to assume that the value of r is small enough in the proposed system and the system response under different initial conditions will be identical.

3.2 Influence of the harmonic excitation frequency

In the simulations presented in Subsection 3.1, the frequency of the harmonic excitation was set to $f_0 = 2$ Hz. However, the excitation frequency in various applications can vary significantly, from low frequency of 2-5 Hz (walking person) to hundreds and thousands of hertz (rotating/moving machines/components). Thus, the device performance under a range of excitation frequencies is studied and presented in this subsection.

To study the response of the system as a function of f_0, the value of A should be kept constant. The curves of U_{ave} and $\langle U \rangle_T$ versus f_0 under different angles are plotted in Figures 6(a, b), where $A = 5$ N and $r = 0.75$. It can be seen from Figure 6(a) that the trend of the U_{ave} curves is complicated. At first, all the curves oscillatory ascending as f_0 increases at a small frequency range and attain their peaks at some f_0 value. Within this range of frequencies, the difference between the curves is quite small indicating that the output performance of the proposed device is not affected by the angle. After achieving their maximum all curves plunge to a much lower level and present a generally decrease trend, except of some discrete points. In Figure 6(b), all $\langle U \rangle_T$ curves have a trend similar to the U_{ave} curves but with much smaller oscillations. One can also see that $\langle U \rangle_T$ has the largest value under $\beta = 90°$ within the high frequency range ($f_0 > 31$ Hz), indicating that within this frequency range the proposed device has optimal output performance when it is installed vertically.

It is worth mentioning that at some discrete frequency points some particular device arrangements with respect to its angle are more beneficial than others. For instance, in Figure 6(a) one can see that at around 29 Hz the horizontal device $\beta = 0°$ will provide the best performance, whereas for 25 Hz the angle should be $\beta = 45°$ and at 30 Hz it should be $\beta = 30°$.

Two curves U_{ave} and $\langle U \rangle_T$ are presented in Figures 6(c-f) for smaller values of r, namely $r = 0.5$ in Figures 6 (c,d) and $r = 0.25$ in Figures 6(e,f). Although all the curves have a similar trend as stated previously, there are some differences. The curves attain their peaks at smaller values of the frequency and the absolute values of the peaks are also smaller. At this point we can return to the question related to the device performance at various values of r and compare Figure 6(a) and (c) and (e). It is clear that at approximately 19 Hz the horizontal device will generate more power at $r = 0.25$ than at $r = 0.5$ or $r = 0.75$. It is believed that the reason for this is the phase difference between the ball and the cylinder at small values of *r*, which changes the ball velocity after each impact and thus influences the time of free motion of the ball between the impacts.

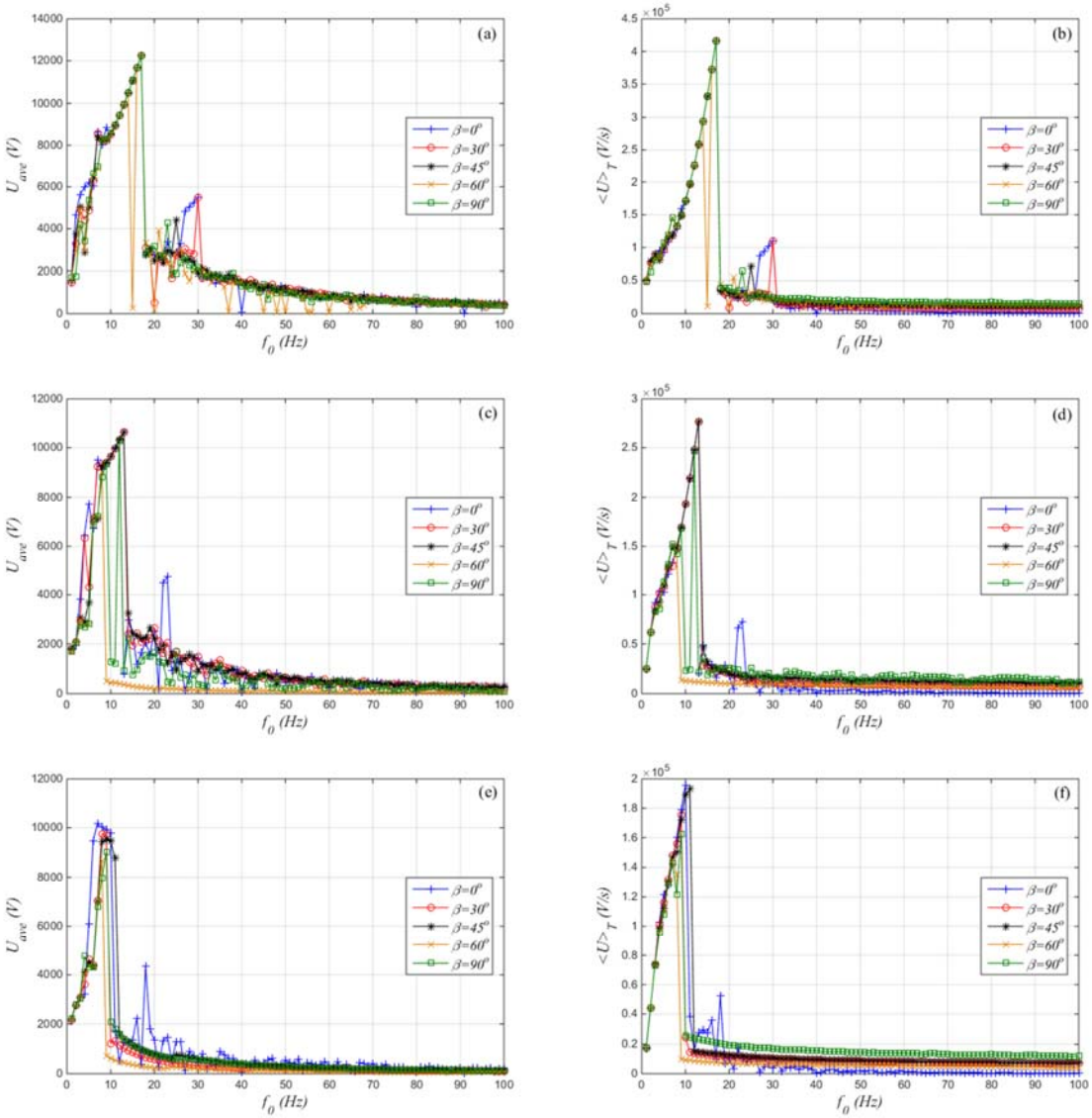

Figure 6. Output voltage for $A = 5$ N; U_{ave} for $r = 0.75$ (a), $r = 0.5$ (c) and $r = 0.25$ (e); $\langle U \rangle_T$ for $r = 0.75$ (b), $r = 0.5$ (d) and $r = 0.25$ (f).

Figure 7 presents similar curves for the excitation amplitude A=20 N. It can be seen that all curves have a similar pattern as those in Figure 6, with higher peak values and higher values of the peaks' frequencies. All curves before their peak values (within the low frequency range) almost coincide, thus the device will produce the same amount of energy at any angle. It should be said that the overall structure of the curves with the drop in the response amplitude reminds the behavior of a forced system with a nonlinear stiffness like a Duffing oscillator.

Figures 6 and 7 can only help in designing the device based on the given excitation frequency, but they cannot explain why the curves demonstrate such a complicated trend. To understand the device performance the bifurcation diagrams of the dynamic system as a function of f_0 for $\beta = 0°$ and $\beta = 90°$ under different values of A and r are presented in Figures 8 and 9.

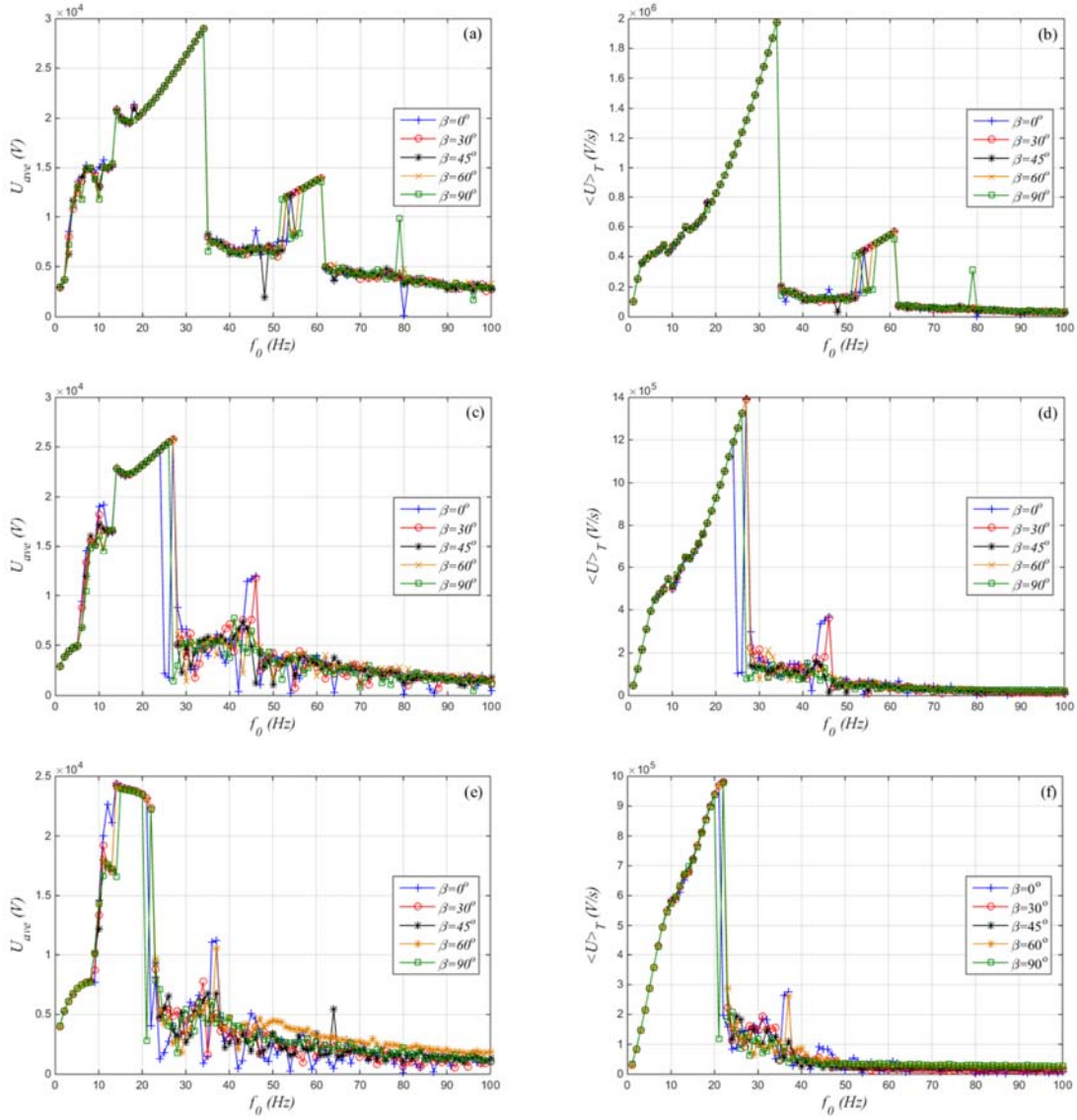

Figure 7. Output voltage for $A = 20$ N; U_{ave} for $r = 0.75$ (a), $r = 0.5$ (c) and $r = 0.25$ (e); $\langle U \rangle_T$ for $r = 0.75$ (b), $r = 0.5$ (d) and $r = 0.25$ (f).

The plots show the relative steady-state velocities difference Δv between the cylinder and the ball just before impact, which determines the value of δ according to (8) and the output voltage U_{imp}; the larger Δv the larger δ and U_{impact}. In these plots one can see a range of Δv values for each and every value of the excitation frequency; moreover, in some cases this range has a couple of discrete values of the relative velocity whereas in other cases a whole range of values is possible, including very small velocities. If one compare these plots to the corresponding plots of output voltage one can see that when small impact velocities are possible, the values of output voltage are relatively small, which can be seen in the case of "high" excitation frequencies. When there are only a couple of high velocity values are available, as can be seen in the "low" frequency range, then the output voltage is high due to high membrane deformation.

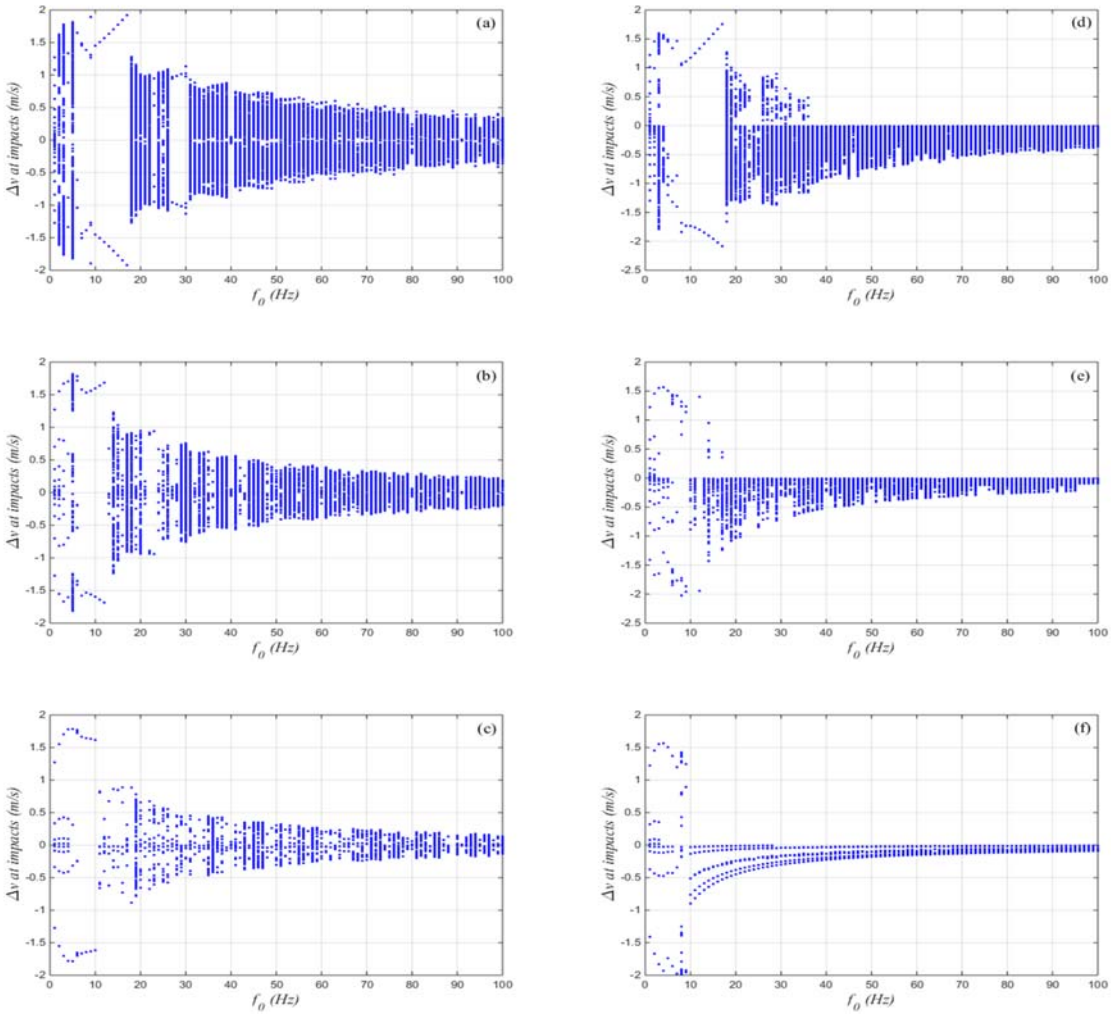

Figure 8. Bifurcation diagrams of the relative impact velocity for A=5 N, $\beta = 0°$, $r = 0.75$ (a), $r = 0.5$ (b), $r = 0.25$ (c); $\beta = 90°$, $r = 0.75$ (d), $r = 0.5$ (e), $r = 0.25$ (f).

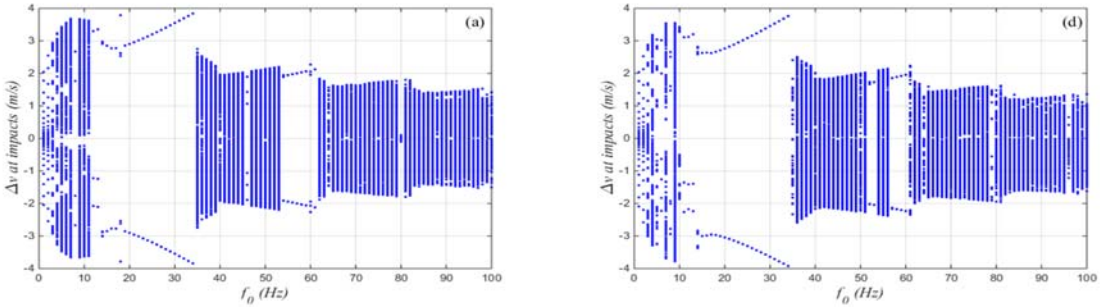

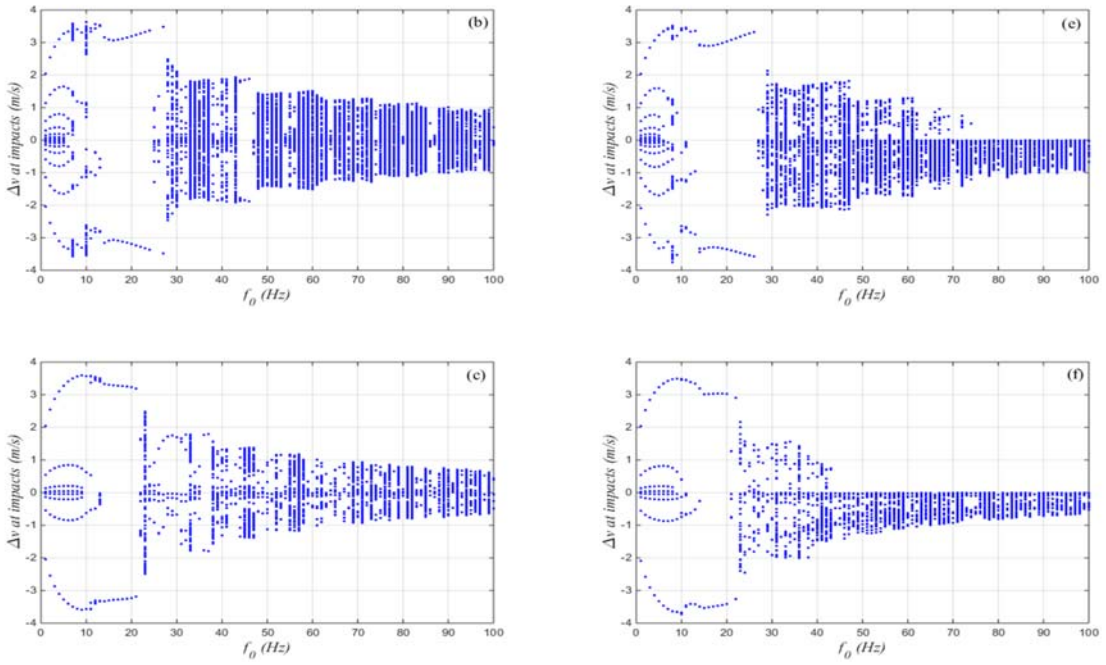

Figure 9. Bifurcation diagrams of the relative impact velocity for A=20 N, $\beta = 0°$, $r = 0.75$ (a), $r = 0.5$ (b), $r = 0.25$ (c); $\beta = 90°$, $r = 0.75$ (d), $r = 0.5$ (e), $r = 0.25$ (f).

One can also see that the plots are symmetric in the case of horizontal device $\beta = 0°$ and asymmetric for the vertical device $\beta = 90°$. The asymmetry reflects the fact that the top membrane cannot always be reached by the ball at low excitation amplitude, when one compares Figure 8 and Figure 9 correspondingly, or high excitation frequency.

3.3 Influence of the excitation amplitude

The amplitude of the harmonic excitation is another important factor that influences the system dynamics. The harmonic excitation $F(t) = A\cos(2\pi f_0 t)$ applied to the system results in the response amplitude of the cylinder's movement that is equal to $A / M(2\pi f_0)^2$. For the convenience and future design of the device let's introduce a non-dimensional parameter:

$$\gamma = \frac{A / [M(2\pi f_0)^2]}{s / 2} \tag{21}$$

Thus, to study the response of the system as a function of γ, the value of f_0 should be kept constant. The curves of U_{ave} and $\langle U \rangle_T$ versus γ under different angles are plotted in Figure 10 for $f_0 = 2$ Hz and $r = 0.75$. Similar curves U_{ave} and $\langle U \rangle_T$ for γ=0.5 and γ=0.25 are plotted in Figure 13, with all other parameters the same as in Figure 10. It can be seen from Figure 10(a) that with an increase of γ all curves can be roughly divided into two parts: the low values of γ range ($0 < \gamma < 28$ for β=0°) and the large values of γ range ($\gamma \geq 28$ for β=0°). All curves demonstrate an increasing trend following a "standard curve", shown in Figures 10 and Figure 13 as red dashed lines. When other curves reach the "standard curve" the difference between various curves

becomes quite small, which indicates that the values of β have little or no influence on the system output performance in the case of large γ. As one can see in Figure 10(a), the curves corresponding to larger angles join the "standard curve" later, i.e. at larger values of γ. The curves shown in Figure 10(b) have a simpler pattern with small oscillations. As γ increases the curves show an upward trend, which is well expected since larger values of γ and, therefore, A mean more energy input into the system resulting in a higher relative acceleration and velocity of impacts. Hence, the strength of the harmonic excitation has a positive effect on the magnitudes of the electrical energy converted through this device. The "standard curve" has been approximated and can be expressed as $\langle U \rangle_T = 3.0 \times 10^4 \cdot \gamma^{0.55}$.

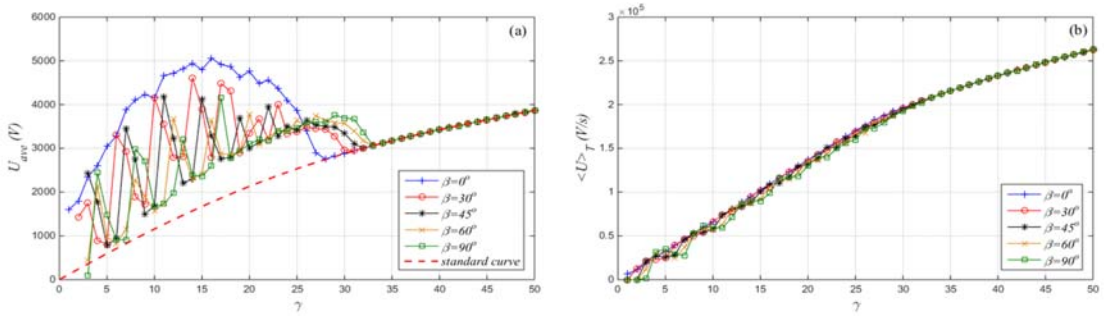

Figure 10. Output voltage curved U_{ave} (a) and $\langle U \rangle_T$ (b) for $f_0 = 2$ Hz and $r = 0.75$.

It is a very interesting phenomenon that the $\langle U \rangle_T$ curves show an increasing trend whereas the U_{ave} curves show an oscillatory pattern before they reach the "standard curve". In order to explain this phenomenon, two special cases of $\beta = 0°$, $\gamma = 15$ and $\gamma = 35$ are chosen from Figure 10 to show the difference in the system responses, as shown in Figures 11 and 12, respectively. In the first case of $\gamma = 15$, the relative displacement between the ball and the cylinder is presented in Figure 11(a), and the displacement of the ball and its limited positions are presented in Figure 11(b) to demonstrate the impact details. After impacting the left membrane at point 1 (Figure 11(b)) both of them move rightward until the cylinder start slowing down whereas the ball keeps moving with its maximum velocity until it reaches the right membrane, indicated by point 2. It should be noted that the cylinder still moves to the right gradually slowing down, so that the ball reaches it again at point 3. Then the cylinder stops completely and starts moving leftward accelerating. The cylinder's velocity increases so the right membrane is able to impact the ball at points 4~6 until the ball is pushed by the right membrane, then the process approximately repeats itself so that the ball's motion presents a quasi-periodic state, shown in Figure 11(c).

The results of the other case with $\gamma = 35$ are presented in Figure 12. It can be seen from Figure 12(a) that initially the curve is a horizontal line, which indicates that the ball stays at the left membrane and moves rightward pushed by the membrane until the cylinder reaches its largest velocity at point 1. After that, the ball moving faster than the cylinder impacts the right membrane at point 2 and then at points 3~5 catching up with the moving rightward right membrane. The cylinder moves reversely after that, reaches its largest displacement and the right membrane with the ball starts moving leftwards accelerating the ball. The process then repeats itself so that the ball's motion is fully periodic as shown in Figure 12(c). However, many low-power generated impacts will occur when the

ball chases the membrane, thus the number of impacts increases in (20) leading to lower values of U_{ave} within the range of larger values of γ than that within the range of small values of γ, although the overall energy gain increases as γ increases.

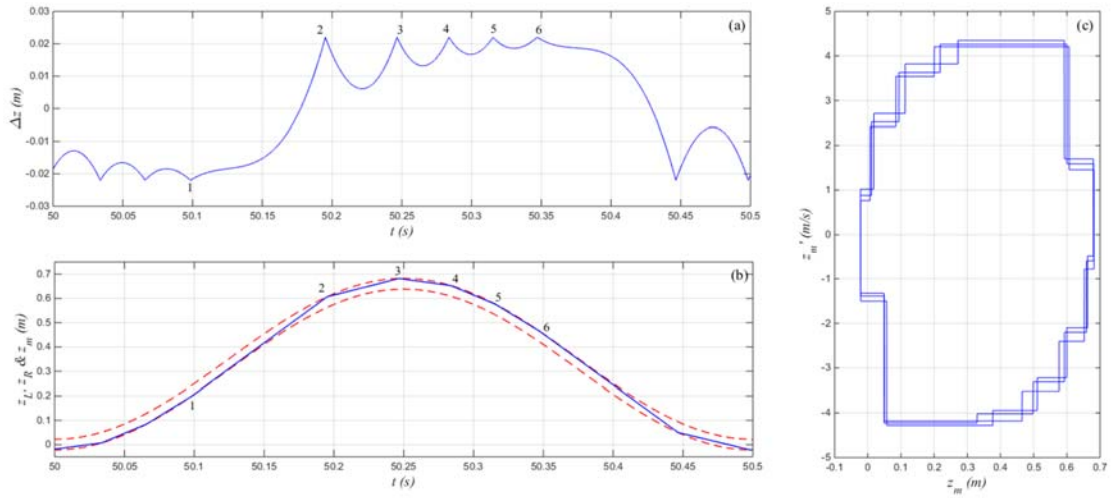

Figure 11. (a) Relative displacement between the ball and cylinder, (b) ball's position and (c) ball's phase trajectory under γ=15 . $f_0 = 2$ Hz, $r = 0.75$.

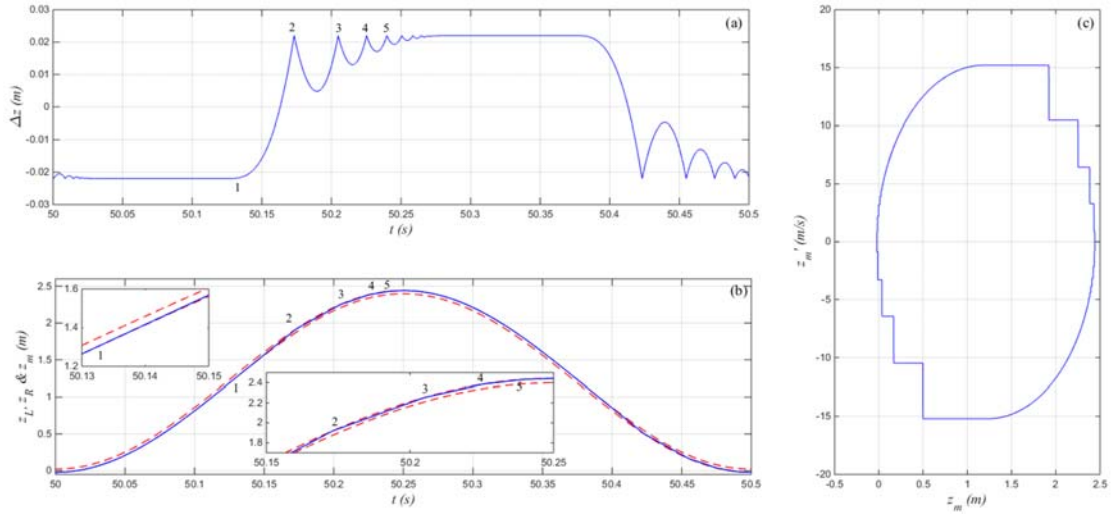

Figure 12. (a)Relative displacement between the ball and cylinder, (b) ball's position and (c) ball's phase trajectory under γ=35 . $f_0 = 2$ Hz, $r = 0.75$.

According to the above analysis, there is a critical value γ_{cr} in the U_{ave} curves that divides the range of γ so that, when $\gamma > \gamma_{cr}$, the system steady state response is periodic and follows the "standard curve", whereas for $\gamma < \gamma_{cr}$, the system steady state response can be quasi-periodic or irregular. The value of γ_{cr} depends on the angle β. When β is large the cylinder needs a larger excitation amplitude to overcome the ball's gravity component so that the right (top) membrane can

be caught up with the ball. Therefore, the γ_{cr} has a positive relationship with β, which is demonstrated in Figure 10(a).

It can be seen that the curves in Figure 13 have a similar pattern compared to those in Figure 10, and the value of γ_{cr} for the same angle decreases as r decreases indicating that the ball's motion pattern converges faster to the "standard curve". Two "standard curves" have been obtained from these results, connecting the output voltage and γ for the case of $r = 0.5$ $\langle U \rangle_T = 2.0 \times 10^4 \cdot \gamma^{0.4824}$ and $r = 0.25$ $\langle U \rangle_T = 1.4 \times 10^4 \cdot \gamma^{0.4652}$, correspondingly.

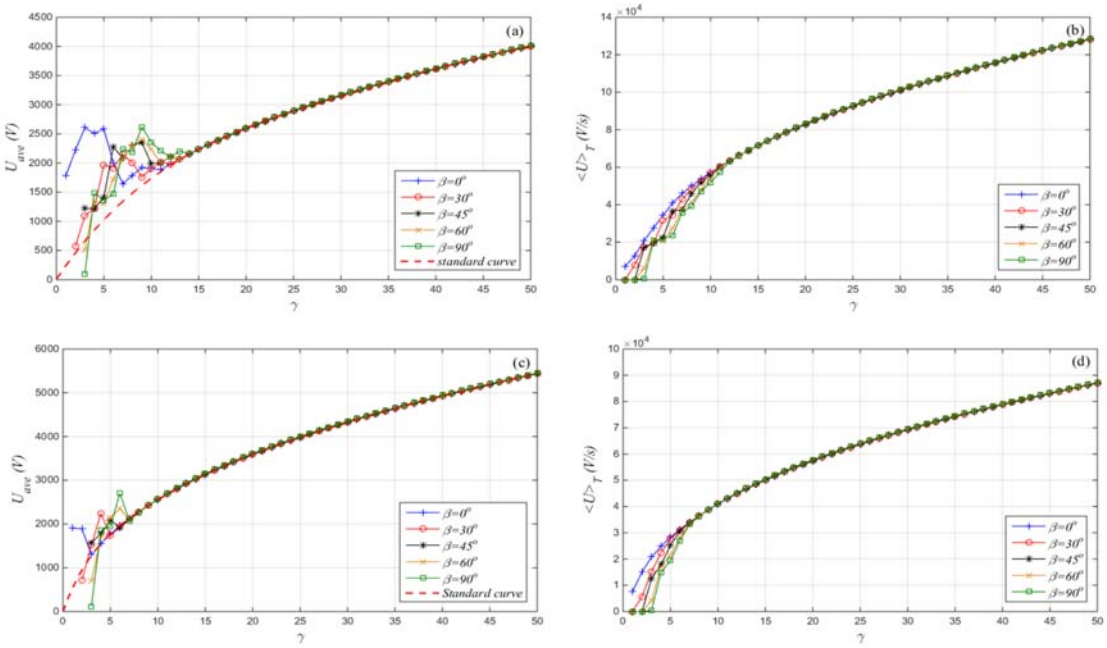

Figure 13. U_{ave} curves for $r = 0.5$ (a) and $r = 0.25$ (c), and $\langle U \rangle_T$ curves for $r = 0.5$ (b) and $r = 0.25$ (d) with $f_0 = 2$ Hz.

Comparing Figures 10(b) and 13(b, d) one can see that the amount of $\langle U \rangle_T$ decreases as r decreases at a same value of γ, indicating that a smaller r will result in more energy dissipation and less harvested energy in general. However, the comparison between different standard curves presents a different law. The standard curves for different r are presented in Figure 14, where one can see that the amount of U_{ave} increases as r decreases at the same value of γ, which can be explained in a similar manner as before by a high number of low-energy impacts at this excitation frequency.

It should be pointed out that large values of γ require either a large A or a low f_0 under a given set of system parameters. Although these conditions are rarely met in machines, where adverse vibrations are properly mitigated, and therefore response along the standard curve is hard to encounter, in a realistic environment it is possible to observe, for instance in ocean waves, which may have a high amplitude and always have a low frequency.

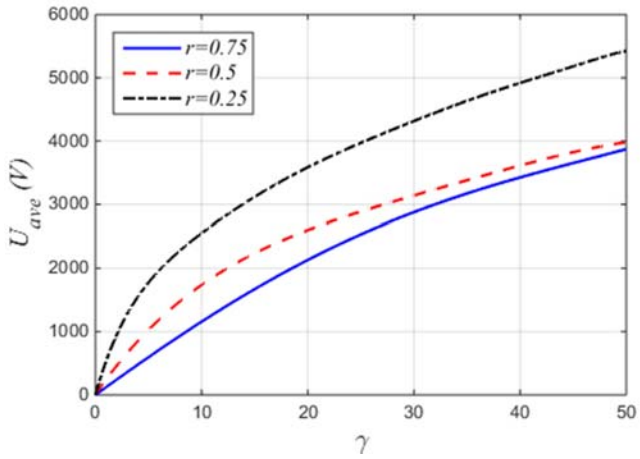

Figure 14. Standard curves of U_{ave} versus γ under different r.

4 Discussion

The study of the EH performance under a harmonic excitation is helpful to understand the rich nonlinear behavior of the proposed device with the given system parameters. In a realistic vibrational environment, where the amplitude and frequency of the excitation are given, the device design can be optimized for its best performance through simulations.

To optimize the design of a real EH device, it is necessary to determine the values of the system parameters, such as M, m, R_0 (R_{cin}), h_0, r_b, d, w and β. Among these parameters, the values of R_0 and h_0 should be fixed first so that one could obtain the parameters of the DE membrane in simulations, such as K, n and r; the values of R_{cin} and r_b are determined accordingly. Thus, for given ball mass and outer structure, the optimization of the EH device can be seen as the optimization of its length (i.e. the distance between two membranes $l = d + 2w$) and angle (β). The optimization procedure of the proposed EH device subjected to a given vibrational environment is given as follows:

Step 1: Measure the vibrations in a given vibrational environment such as human walking, ambient vibrations near machines, etc., and obtain the approximate maximum value of the excitation amplitude and peak (mean) frequency;

Step 2: Choose l and β as variables and calculate the average gained voltage $\langle U \rangle_T$ of the proposed device at its steady state under different values of l and β;

Step 3: Acquire the maximal value of $\langle U \rangle_T$. The corresponding values of l and β are the best parameters of the proposed device for working in the given vibrational environment.

A specific case to optimize the design of the proposed EH device mounted onto a car engine compartment is given below to further demonstrate the optimization procedure. The peak acceleration (A/M) is 12 m/s^2 and the peak frequency (f_0) is 200 Hz in a car engine compartment[61] and it is assumed that this acceleration is the same in all direction. Assuming that $r = 0.5$, and all parameters, except d, w and β, are kept constant and set as the values in the previous simulations, the $\langle U \rangle_T$ versus l curves under different angles ($0°$, $30°$, $45°$, $60°$ and $90°$) are presented in Figure 15(a),

where the value of l varies from 10 mm to 20 mm and real-ICs are imposed in all the simulations. It can be seen from Figure 15 that as l increases:

1. The values of $\langle U \rangle_T$ vary within a relatively small range when β=0°, and the maximal value is obtained when $l = 11$ mm as shown in the built-in plot.

2. The $\langle U \rangle_T$ curves present a similar horizontal trend when l > 11 mm at β=30°, 45°, 60°, indicating that the average output voltage gain has nothing to do with the length of the cylinder, because impacts only occur at the left (bottom) membrane due to the small excitation amplitude, thus the degrees of impacts are decided by the gravity component. The maximal value of $\langle U \rangle_T$ is achieved when β=30°.

According to the above analyses, to achieve the best EH performance for the car engine compartment, the length of the cylinder ($l = d + 2w$) should be chosen as 11 mm, so that most energy can be harvested at any angle, and it is better to set the device inclined at an angle of 30° if possible. Thus, the optimized EH device will produce $\langle U \rangle_T$ =4679 V/s. The power generated by this device[59] can be further obtained: $P = \frac{1}{2} C_0 U_{in} \langle U \rangle_T = 0.0702$ mW. Here, $C_0 = \varepsilon_0 \varepsilon_r A_0 / h_0 = 1.5 \times 10^{-11}$ F, where $\varepsilon_0 = 8.85 \times 10^{-12}$ F/m, $\varepsilon_r = 3.4$.

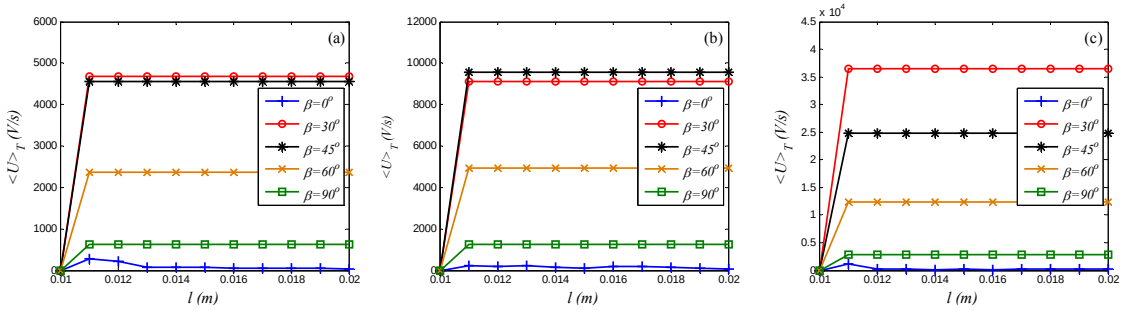

Figure 15. Output performance of the proposed device under different l and for a car engine compartment. (a) $m = 3.5$ g; (b) $m = 12.45$ g; (c) $m = 62.25$ g.

It can be learned from (8) that a larger value of m produces a larger δ, therefore, a larger output voltage at each impact. Thus, it is possible to further improve the EH performance of the proposed device through increasing the mass of the ball with other parameters kept unchanged. It should be first noticed that when m is large, (16) should be used to calculate the velocity of the ball after impacts. Two optimization figures for the proposed device with $m = 12.45$ g (μ=0.1) and $m = 62.25$ g (μ=0.5) are presented in Figures 15(b, c), respectively. It can be seen that all the $\langle U \rangle_T$ curves have the familiar pattern as those in Figure 15(a).

The optimal angles for different m and the relevant values of maximum $\langle U \rangle_T$ and maximal power are summarized in Table 2. It can be seen that the optimal EH performance of the proposed device is improved with increasing the values of m. However, because the largest deformation δ of the membranes at impacts is not proportional to the value of m, this positive relationship is not linear. For example, with the value of m increasing nearly four times from 3.5 g to 12.45 g, the maximal power only increases about two times. Therefore, it is possible to increase the amount of harvested

energy by increasing the ball mass, however, larger mass makes the device heavier, bigger, and eventually may break the membrane.

Table 2. Optimal angles for different m and the values of maximal $\langle U \rangle_T$ and maximal power.

m (g)	3.5	12.45	62.25
Optimal angle (°)	30	45	30
Maximal $\langle U \rangle_T$ (V/s)	4557	9560	36420
Maximal power (mW)	0.0702	0.143	0.547

5 Conclusions

In this paper a DE-based energy harvesting device has been presented and analyzed. The concept is based on the VI motion of a ball, moving freely inside a capsule (cylinder), both sides of which are covered by DE membranes. The dynamic analysis was conducted first, and the membrane deformation under external excitation was analyzed analytically in connection to the amount of voltage that can be generated. Thus, the basic principle of energy harvesting based on the proposed device under external excitation was introduced. The dynamic response of the system is rich and colorful. By taking two evaluation indexes based on output voltage gain, the dynamic and electrical performance of the system depending on initial conditions, angles, restitution coefficient, amplitude and frequency of the harmonic excitation were thoroughly studied and critically analyzed. The study is helpful to optimize the design of the device subjected to a real vibrational environment by adjusting its length and angle to the given excitation parameters. The optimization procedure was discussed, and a specific case of the design optimization for a car engine compartment was presented. The influence of the mass of the ball on the optimal EH performance of the proposed device was studied at last.

Acknowledgement

This work was supported by Jiangxi Provincial Natural Science Foundation (Grant No. 20161BAB216111) and Science & Technology Research Project of Education Department of Jiangxi Province (Grant No. GJJ150068). Zhihui Lai would like to thank the China Scholarship Council for its support (File No. 201606825019).

Reference

[1] Daqaq M F, Masana R, Erturk A, Quinn D D. On the role of nonlinearities in vibratory energy harvesting: a critical review and discussion. Applied Mechanics Reviews, 2014, 66(4): 040801.

[2] Inki Jung, Youn-Hwan Shin, Sangtae Kim, Ji-young Choi, Chong-Yun Kang. Flexible piezoelectric polymer-based energy harvesting system for roadway applications. Applied Energy, 2017, 197: 222-229.

[3] Bowen C R, Arafa M H. Energy harvesting technologies for tire pressure monitoring systems. Advanced Energy Materials, 2015, 5(7).

[4] Le M Q, Capsal J F, Lallart M, Hebrard Y, Ham A V D, Reffe N, Geynet L, Cottinet P. Review on energy harvesting for structural health monitoring in aeronautical applications. Progress in Aerospace Sciences, 2015, 79: 147-157.

[5] Mckay T G, Rosset S, Anderson I A, Shea H. Dielectric elastomer generators that stack up. Smart Materials and Structures, 2014, 24(1): 015014.

[6] Tan Y K, Panda S K. Review of energy harvesting technologies for sustainable wireless sensor network. Sustainable wireless sensor networks, 2010: 15-43.
[7] Shuai Wu, P.C.K Luk, Chunfang Li, Xiangyu Zhao, Zongxia Jiao, Yaoxing Shang. An electromagnetic wearable 3-DoF resonance human body motion energy harvester using ferrofluid as a lubricant. Applied Energy, 2017, 197: 364-374.
[8] Bowen C R, Kim H A, Weaver P M, Dunn S. Piezoelectric and ferroelectric materials and structures for energy harvesting applications. Energy & Environmental Science, 2014, 7(1): 25-44.
[9] Chen Z, Guo B, Yang Y, Cheng C. Metamaterials-based enhanced energy harvesting: A review. Physica B: Condensed Matter, 2014, 438: 1-8.
[10] Matiko J W, Grabham N J, Beeby S P, Tudor M J. Review of the application of energy harvesting in buildings. Measurement Science and Technology, 2013, 25(1): 012002.
[11] Xiang Wang, Changsong Chen, Na Wang, Haisheng San, Yuxi Yu, Elinar Halvorson, Xuyuan Chen. A frequency and bandwidth tunable piezoelectric vibration energy harvester using multiple nonlinear techniques. Applied Energy, 2017, 190: 368-375.
[12] Shengxi Zhou, Junyi Cao, Daniel J. Inman, Jing Lin, Shengsheng Liu, Zezhou Wang. Broadband tristable energy harvester: Modeling and experiment verification. Applied Energy, 2014, 133: 33-39.
[13] Santiago Orrego, Kourosh Shoele, Andre Ruas, Kyle Doran, Brett Caggiano, Rajat Mittal. Harvesting ambient wind energy with an inverted piezoelectric flag. Applied Energy, 2017, 194: 212-222.
[14] Leng Y G, Gao Y J, Tan D, Fan S B, Lai Z H. An elastic-support model for enhanced bistable piezoelectric energy harvesting from random vibrations. Journal of Applied Physics, 2015, 117(6): 064901.
[15] Gao Y, Leng Y, Javey A, Tan D, Liu J, Fan S, Lai Z. Theoretical and applied research on bistable dual-piezoelectric-cantilever vibration energy harvesting toward realistic ambience. Smart Materials and Structures, 2016, 25(11): 115032.
[16] Huang J, Shian S, Suo Z, Clarke D R. Maximizing the Energy Density of Dielectric Elastomer Generators Using Equi-Biaxial Loading. Advanced Functional Materials, 2013, 23(40): 5056-5061.
[17] Kang G, Kim K S, Kim S. Note: Analysis of the efficiency of a dielectric elastomer generator for energy harvesting. Review of Scientific Instruments, 2011, 82(4): 046101.
[18] Li T, Qu S, Yang W. Energy harvesting of dielectric elastomer generators concerning inhomogeneous fields and viscoelastic deformation. Journal of Applied Physics, 2012, 112(3): 034119.
[19] Bortot E, Gei M. Harvesting energy with load-driven dielectric elastomer annular membranes deforming out-of-plane. Extreme Mechanics Letters, 2015, 5: 62-73.
[20] McKay T G, O'Brien B M, Calius E P, Anderson I A. Soft generators using dielectric elastomers. Applied Physics Letters, 2011, 98(14): 142903.
[21] Jean-Mistral C, Vu Cong T, Sylvestre A. Advances for dielectric elastomer generators: Replacement of high voltage supply by electret. Applied Physics Letters, 2012, 101(16): 162901.
[22] Xiongfei Liu, Liwu Liu, Yanju Liu, Jinsong Leng. Dielectric elastomer energy harvesting: maximal converted energy, viscoelastic dissipation and a wave power generator. Smart Materials and Structures, 2015, 24(11): 115036.
[23] Pelrine R, Kornbluh R D, Eckerle J, Jeuck P, Oh S, Pei Q, Stanford S. Dielectric elastomers: generator mode fundamentals and applications//SPIE's 8th Annual International Symposium on Smart Structures and Materials. International Society for Optics and Photonics, 2001: 148-156.

[24] Suo Z, Zhao X, Greene W H. A nonlinear field theory of deformable dielectrics. Journal of the Mechanics and Physics of Solids, 2008, 56(2): 467-486.
[25] Schmidt A, Rothemund P, Mazza E. Multiaxial deformation and failure of acrylic elastomer membranes. Sensors and Actuators A: Physical, 2012, 174: 133-138.
[26] Koh S J A, Keplinger C, Li T, Bauer S. Dielectric elastomer generators: How much energy can be converted?. IEEE/ASME Transactions on mechatronics, 2011, 16(1): 33-41.
[27] Tröls A, Kogler A, Baumgartner R, Kaltsels R, Keplinger C, Schwödiauer R, Graz I, Bauer S. Stretch dependence of the electrical breakdown strength and dielectric constant of dielectric elastomers. Smart Materials and Structures, 2013, 22: 104012.
[28] Zhu Y, Wang H, Zhao D, Zhao J. Energy conversion analysis and performance research on a cone-type dielectric electroactivepolymer generator. Smart Materials and Structures, 2011, 20(11): 115022.
[29] Graf C, Hitzbleck J, Feller T, Clauberg K, Wagner J, Krause J, Mass J. Dielectric elastomer–based energy harvesting: Material, generator design, and optimization. Journal of Intelligent Material Systems and Structures, 2014, 25(8): 951-966.
[30] Koh S J A, Zhao X, Suo Z. Maximal energy that can be converted by a dielectric elastomer generator. Applied Physics Letters, 2009, 94(26): 262902.
[31] El-Hami M, Glynne-Jones P, White N M, Hill M, Beeby S. Design and fabrication of a new vibration-based electromechanical power generator. Sensors and Actuators A: Physical, 2001, 92(1): 335-342.
[32] Despesse G, Jager T, Jean-Jacques C, Leger J, Vassilev A, Basrour S, Charlot B. Fabrication and characterization of high damping electrostatic micro devices for vibration energy scavenging. Proc. Design, Test, Integration and Packaging of MEMS and MOEMS. 2005: 386-390.
[33] Roundy S, Wright P K, Rabaey J. A study of low level vibrations as a power source for wireless sensor nodes. Computer communications, 2003, 26(11): 1131-1144.
[34] Chiba S, Waki M, Wada T, Hirakawa Y, Masuda K, Ikoma T. Consistent ocean wave energy harvesting using electroactive polymer (dielectric elastomer) artificial muscle generators. Applied Energy, 2013, 104: 497-502.
[35] Moretti G, Forehand D, Vertechy R, Fontana M, Ingram D. Modeling of an oscillating wave surge converter with dielectric elastomer power take-off. ASME 2014 33rd International Conference on Ocean, Offshore and Arctic Engineering, 2014: OMAE2014-23559.
[36] Bobryk R V, Yurchenko D. On enhancement of vibration-based energy harvesting by a random parametric excitation. Journal of Sound and Vibration, 2016, 366: 407-417.
[37] Quinn D D, Triplett A L, Bergman L A, Vakakis A F. Comparing linear and essentially nonlinear vibration-based energy harvesting. Journal of vibration and acoustics, 2011, 133(1): 011001.
[38] Ibrahim R A. Vibro-impact dynamics: modeling, mapping and applications. Springer Science & Business Media, 2009.
[39] Dimentberg M F, Iourtchenko D V. Random vibrations with impacts: a review. Nonlinear Dynamics, 2004, 36(2): 229-254.
[40] Iourtchenko D V, Song L L. Numerical investigation of a response probability density function of stochastic vibroimpact systems with inelastic impacts. International Journal of Non-Linear Mechanics, 2006, 41(3): 447-455.
[41] Fidlin A. Nonlinear oscillations in mechanical engineering. Springer Science & Business Media, 2005.

[42] Bendame M, Abdel-Rahman E, Soliman M. Wideband, low-frequency springless vibration energy harvesters: part I. Journal of Micromechanics and Microengineering, 2016, 26(11): 115021.
[43] Bendame M, Abdel-Rahman E, Soliman M. Wideband, low-frequency springless vibration energy harvesters: part II. Journal of Micromechanics and Microengineering, 2016, 26(11): 115022.
[44] Babitsky V I. Theory of vibro-impact systems and applications. Springer Science & Business Media, 2013.
[45] Pavlovskaia E, Hendry D C, Wiercigroch M. Modelling of high frequency vibro-impact drilling. International Journal of Mechanical Sciences, 2015, 91: 110-119.
[46] Masri S F, Caughey T K. On the stability of the impact damper. Journal of Applied Mechanics, 1966, 33(3): 586-592.
[47] Al-Shudeifat M A, Wierschem N, Quinn D D, Vakakis A F, Bergman L A, Spencer Jr. B F. Numerical and experimental investigation of a highly effective single-sided vibro-impact non-linear energy sink for shock mitigation. International journal of non-linear mechanics, 2013, 52: 96-109.
[48] Gendelman O V, Alloni A. Dynamics of forced system with vibro-impact energy sink. Journal of Sound and Vibration, 2015, 358: 301-314.
[49] Li T, Gourc E, Seguy S, Berlioz A. Dynamics of two vibro-impact nonlinear energy sinks in parallel under periodic and transient excitations. International Journal of Non-Linear Mechanics, 2017, 90: 100-110.
[50] Blazejczyk-Okolewska B, Czolczynski K, Kapitaniak T. Classification principles of types of mechanical systems with impacts–fundamental assumptions and rules. European Journal of Mechanics-A/Solids, 2004, 23(3): 517-537.
[51] Makarenkov O, Lamb J S W. Dynamics and bifurcations of nonsmooth systems: A survey. Physica D: Nonlinear Phenomena, 2012, 241(22): 1826-1844.
[52] Jacquelin E, Adhikari S, Friswell M I. A piezoelectric device for impact energy harvesting. Smart Materials and Structures, 2011, 20(10): 105008.
[53] Halim M A, Khym S, Park J Y. Frequency up-converted wide bandwidth piezoelectric energy harvester using mechanical impact. Journal of Applied Physics, 2013, 114(4): 044902.
[54] Moss S, Barry A, Powlesland I, Galea S, Carman G P. A low profile vibro-impacting energy harvester with symmetrical stops. Applied Physics Letters, 2010, 97(23): 234101.
[55] Borowiec M, Litak G, Lenci S. Noise effected energy harvesting in a beam with stopper. International Journal of Structural Stability and Dynamics, 2014, 14(08): 1440020.
[56] Afsharfard A. Application of nonlinear magnetic vibro-impact vibration suppressor and energy harvester. Mechanical Systems and Signal Processing, 2018, 98: 371-381.
[57] Guo Y. Bifurcation and chaos of nonlinear vibro-impact systems. PhD Thesis, 2013.
[58] Pierański P, Barberi R. Bouncing Ball Workbench. 1994.
[59] Yurchenko D, Val D V, Lai Z H, Gu G, Thomson G. Energy harvesting from a DE-based dynamic vibro-impact system. Smart Materials and Structures. (To appear).
[60] Yurchenko D, Lai Z H, Thomson G, Val D V, Bobryk R. Parametric study of a novel vibro-impact energy harvesting system with dielectric elastomer. Applied Energy. (Under review)
[61] Nechibvute A, Chawanda A, Luhanga P. Piezoelectric energy harvesting devices: an alternative energy source for wireless sensors. Smart Materials Research, 2012: 853481.